Available online at www.sciencedirect.com
ScienceDirect
Journal of the European Ceramic Society 28 (2008) 2337–2343
www.elsevier.com/locate/jeurceramsoc

Crack propagation in directionally solidified eutectic ceramics

L. Perrière [a,b], R. Valle [a,*], L. Mazerolles [b], M. Parlier [a]

[a] *ONERA/DMSC, 29 avenue de la Division Leclerc, F-92322 Châtillon Cedex, France*
[b] *CNRS/CECM, 15 rue G. Urbain, F-94407 Vitry-sur-Seine Cedex, France*

Available online 4 March 2008

Abstract

Improving the strength and toughness of directionally solidified eutectic ceramics is essential for practical applications. In this respect, a biaxial disc flexure testing device has been designed. This system, which presents the ring supported/ring loaded test geometry, is essentially used as a means for the nucleation and early propagation of cracks, with the flexure test being stopped as soon as a load drop is detected in the loading curve. The composites under investigation are either binary ($Al_2O_3/Y_3Al_5O_{12}$, $Al_2O_3/Er_3Al_5O_{12}$ and $Al_2O_3/GdAlO_3$) or ternary ($Al_2O_3/Y_3Al_5O_{12}/ZrO_2$, $Al_2O_3/Er_3Al_5O_{12}/ZrO_2$ and $Al_2O_3/GdAlO_3/ZrO_2$) eutectics. Examination of cracks is performed in field emission gun-scanning electron microscope on the polished surface of the biaxial bending test specimens, with attention being paid to the possibility of crack deflection in the various phases and in the phase boundaries, a phenomenon which may markedly improve the toughness of these eutectic ceramics. These observations are correlated to internal stress calculations, such as normal stress acting on the phase boundaries.

Keywords: Eutectic ceramics; Interconnected composites; Fracture; Al_2O_3; Rare-earth oxides

1. Introduction

Directionally solidified eutectic ceramics add new potential advantages to sintered ceramics: a higher strength almost constant up to temperatures close to the melting point, and a better creep resistance.[1,2] The microstructure of melt growth composites (MGC) of ceramic oxides consists in three-dimensional and continuous interconnected networks of single-crystal eutectic phases. After solidification of binary eutectics, the eutectic phases are alumina and either a $LnAlO_3$ perovskite phase (Ln, lanthanide element: Gd, Eu) or a $Ln_3Al_5O_{12}$ garnet phase (Ln: Y, Yb, Er, Dy). In the case of ternary systems, zirconia is added as a third phase. In the present case, the directionally solidified eutectic ceramics under investigation are either binary ($Al_2O_3/Y_3Al_5O_{12}$ (YAG), $Al_2O_3/Er_3Al_5O_{12}$ (EAG) and $Al_2O_3/GdAlO_3$ (GAP)) or ternary (Al_2O_3/YAG/ZrO_2, Al_2O_3/EAG/ZrO_2 and Al_2O_3/GAP/ZrO_2) eutectics. However, improving the strength and toughness of eutectic ceramics is essential for practical applications such as turbine blades in future aerospace engines or thermal power generation systems. A better knowledge of the crack propagation modes in such an interconnected microstructure is thus required. In this respect, a biaxial disc flexure testing device has been designed and built at ONERA. The observed crack propagation modes will be correlated to internal stress calculations. The thermal residual stresses found in composite materials result from the thermal expansion mismatch between the different phases. In ceramic eutectics, residual internal stresses measurements have already been performed using either X-ray[3,4] or neutron[5] diffraction techniques and Raman spectroscopy.[6,7] These residual stresses greatly affect the mechanical behaviour of the material. For instance, during tensile or creep tests, the yield stress is attained first in the phases under tension, thus allowing earlier deformation of these phases. Concerning the crack propagation modes, tensile stresses within a phase will act in favor of transverse crack propagation in this phase, whereas a normal tensile stress on the phase boundaries will help interface crack propagation. However, calculation of the internal thermal stresses requires the prior knowledge of the thermomechanical parameters of the various phases[8–12] and of the eutectic composites.[13] In the present investigation, complementary measurements have been performed on the eutectic composites. The determined parameters have allowed the calculation of estimates of these two types of stress components and have helped explain the observed crack propagation modes.

* Corresponding author. Tel.: +33 1 46 73 45 69; fax: + 33 1 46 73 41 42.
E-mail address: roger.valle@onera.fr (R. Valle).

0955-2219/$ – see front matter © 2008 Elsevier Ltd. All rights reserved.
doi:10.1016/j.jeurceramsoc.2008.01.005

Table 1
Chemical compositions and eutectic phases of the investigated *in situ* eutectic composites

Composition (mol%)	Eutectic phases			Ref.
$81Al_2O_3$–$19Y_2O_3$	Al_2O_3	$Y_3Al_5O_{12}$ (YAG)		14
$81Al_2O_3$–$19Er_2O_3$	Al_2O_3	$Er_3Al_5O_{12}$ (EAG)		15
$77Al_2O_3$–$23Gd_2O_3$	Al_2O_3	$GdAlO_3$ (GAP)		14,16
$65Al_2O_3$–$16Y_2O_3$–$19ZrO_2$	Al_2O_3	YAG	ZrO_2	17
$65.9Al_2O_3$–$15.5Er_2O_3$–$18.6ZrO_2$	Al_2O_3	EAG	ZrO_2	18
$58Al_2O_3$–$19Gd_2O_3$–$23ZrO_2$	Al_2O_3	GAP	ZrO_2	19

2. Experimental procedures

2.1. Crystal growth

Eutectic samples are prepared from high purity Al_2O_3 (Baikowski Chimie, France), Y_2O_3 (Rhodia, formerly Rhône Poulenc, France), Er_2O_3 (Rhodia, France), Gd_2O_3 (Rhodia, France) and ZrO_2 (Th. Goldschmidt Industriechemikalien, Germany) powders mixed at the appropriate eutectic compositions (Table 1).[14–19] Rods are isostatically pressed at room temperature and then sintered at 1400 °C for 10 h in order to improve handling strength. Directional solidification is performed in air using the floating-zone translation technique. The various solidification runs are achieved in an arc image furnace operating with a 6 kW xenon lamp as a radiation source, at a solidification rate of 10 mm h^{-1} (20 mm h^{-1} in the case of Al_2O_3/EAG/ZrO_2). Final rods of oriented eutectics are about 8 mm in diameter and 40 mm in length. The solidification oriented eutectic ceramics thus obtained present a fine interconnected microstructure.[19]

2.2. Biaxial flexure testing

The biaxial flexure test offers many advantages over the beam-bending test. First of all, the beam-bending test is influenced by the conditions of the edges parallel to the specimen major axis, the presence of flaws at these edges leading to premature crack initiation, and thus to non-representative strength values. On the contrary, the coaxial-ring test is free of edge condition influences; cracks initiate in the central area and propagate outwardly. The initiation of cracks and the strength values thus only depend on the condition of the specimen surface subjected to the tensile loading and on the bulk homogeneity of the specimen. This possibility to test a relatively large area free from edge finishing defects is a major advantage, other advantages include the ease of specimen preparation and the use of thin sheet material.

The biaxial disc flexure testing device designed and built at ONERA presents the ring supported/ring loaded test geometry (Fig. 1). In this compression testing system, the circular shaped punch is fixed directly on the crosshead of the rigid frame (Fig. 1a). An *x*–*y* adjustment device allows alignment of the punch with the cylindrical specimen holder. Vertical motion and guidance of the specimen holder is ensured through a ball screw, a needle roller thrust bearing and a linear bearing slide. The load cell is fixed on the loading support, flexure plates allowing a friction free displacement between the specimen holder and the loading support. The disc specimen (≈5 mm in diameter, ≈800 μm in thickness) rests freely on the support ring and is loaded coaxially to the support ring with the circular shaped punch (Fig. 1b). Once deflection of the specimen occurs, the flat ended punch acts as a ring loading device (Fig. 1b). Extension of the specimen beyond the support ring eliminates the edge

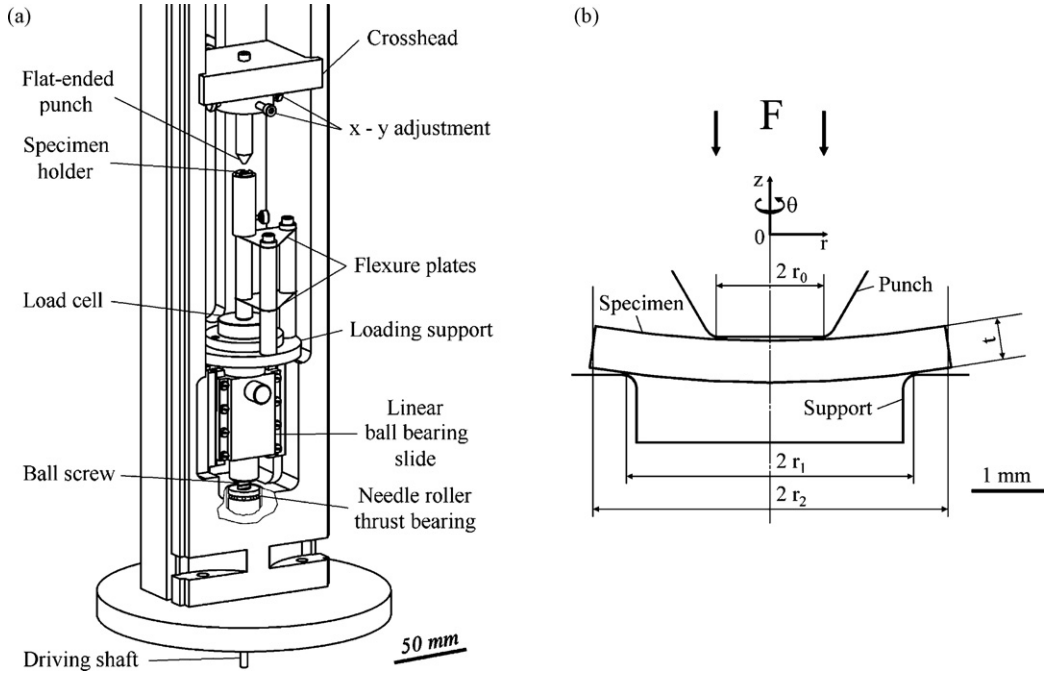

Fig. 1. The biaxial disc flexure testing device (a). The specimen under biaxial loading between the flat-ended punch (radius r_0) and the support (radius r_1), with specimen overhang ($r_2 - r_1$) (b).

effects.[20] The specimen thickness is smaller than the support ring diameter and the specimen deflection is smaller than its thickness, the specimen may thus be considered as a thin rigid plate for which the equations of the theory of elasticity are applicable. The stress components may thus be determined through an analytical calculation[21]; in the central area, inside the inner loading ring ($0 \leq r \leq r_0$), the radial (σ_r) and tangential (σ_θ) stress components are equal, uniform and maximum; they are given by

$$\sigma_r = \sigma_\theta = \frac{3(1+\nu)F}{4\pi t^2}\left[2\ln\frac{r_1}{r_0} + \frac{1-\nu}{1+\nu}\frac{r_1^2 - r_0^2}{r_1^2}\frac{r_1^2}{r_2^2}\right] \quad (1)$$

where F is the applied force, ν the Poisson's ratio of the specimen, r_0 the loading disc radius, r_1 the support ring radius, r_2 the specimen radius and t the specimen thickness. The factor r_1^2/r_2^2 represents the correction for the stiffening effect of the overhang portion of the specimen.

The fact that the biaxial stress system is uniform within the inner loading ring (i.e. over a relatively large area) constitutes another advantage of the coaxial-ring test, since the measured strength of brittle materials depends on the size of the tested area. Moreover, this system being essentially used as a means for the nucleation and early propagation of cracks, the flexure test is stopped as soon as a load drop is detected in the loading curve.

Slices for the biaxial bending tests are cut perpendicular to the growth axis of the 8 mm in diameter eutectic rods, the 5 mm in diameter discs being cut in the central area of the slice. A high quality surface finish of the specimen surface which will be subjected to the biaxial tensile loading (i.e. the lower surface in the present device) is obtained through diamond polishing. The biaxial bending tests are conducted at room temperature. After the flexure tests, examination of cracks is performed in the Zeiss Gemini field emission gun-scanning electron microscope (FEG-SEM).

2.3. Thermomechanical testing

Dilatometric measurements in the longitudinal direction are performed in an Adamel (DI24) thermoanalyser. Eutectic ceramic rods, approximately 8 mm in diameter and 15 mm in length, are used for these measurements, the sample ends being ground flat and parallel. Alumina single crystals, cut parallel or perpendicular to the c axis are used as a calibration test.

Longitudinal compression tests are performed on parallelepipedal specimens, approximately 7 mm × 4 mm × 4 mm, cut parallel to the solidification direction, using a diamond edged blade. The specimens are equipped with strain gauges mounted on two parallel sides. These tests are conducted on an electromechanical MTS (DY 37) testing system, at a rather low stress level (≈150 MPa), i.e. in the elastic domain.

3. Results

3.1. Crack propagation modes

In the six investigated directionally solidified eutectics, the essential propagation mode is the transgranular crack propagation (Fig. 2). A zig-zag crack growth with multiple branches is observed in most cases. However, this type of crack propagation does not only result from deflections of the cleavage crack inside each phase or when crossing phase boundaries, but more essentially from crack deflection in the interfaces themselves. Interface crack propagation is thus observed between Al_2O_3 and YAG (large black arrows in Fig. 2a and b), Al_2O_3 and EAG (large black arrows in Fig. 2c and d), Al_2O_3 and GAP (large black arrows in Fig. 2e and f), Al_2O_3 and ZrO_2 (white arrows in Fig. 2b, d and f), YAG and ZrO_2 (sharp black arrow in Fig. 2b) and EAG and ZrO_2 (sharp black arrow in Fig. 2d). However, interface crack propagation is not observed between GAP and ZrO_2. Crack branching is observed, not only in one of the various phases such as ZrO_2 (split arrow in Fig. 2b), but also in the interfaces where crack deflection through debonding has occurred (split arrows in Fig. 2a, e and f). In most cases, these bifurcation mechanisms lead to stopped cracks (Fig. 2a, b, e and f).

3.2. Thermomechanical behaviour

The thermal expansion curves (strain *vs.* temperature) of Al_2O_3 single crystals (directions // and ⊥ c) and of the investigated binary and ternary eutectic ceramics (longitudinal direction) are reported in Fig. 3. The coefficients of thermal expansion (CTE), which are given by the slope of the curves, are reported in Table 2. The CTEs found for Al_2O_3 (directions // and ⊥ c) agree with those found in the literature. These experimentally determined values, which will be used for the internal stress calculations, confirm the quality of calibration of the thermoanalyser.

Table 2
Coefficients of thermal expansion of Al_2O_3 single crystals (directions // and ⊥ c) and of the investigated eutectic ceramics (longitudinal direction)

	α (10^{-6} K^{-1}) 500 K	α (10^{-6} K^{-1}) 1000 K	α (10^{-6} K^{-1}) 1500 K
Al_2O_3 //c	8.2	9.3	10.5
Al_2O_3 ⊥ c	8	8.7	9.5
Al_2O_3/YAG	8.3	9.1	9.9
Al_2O_3/YAG/ZrO_2	8.4	9.2	10.1
Al_2O_3/EAG	8.2	9	9.3
Al_2O_3/EAG/ZrO_2	8.2	9.3	10.3
Al_2O_3/GAP	8.1	9.1	10
Al_2O_3/GAP/ZrO_2	8.1	9.5	10.9

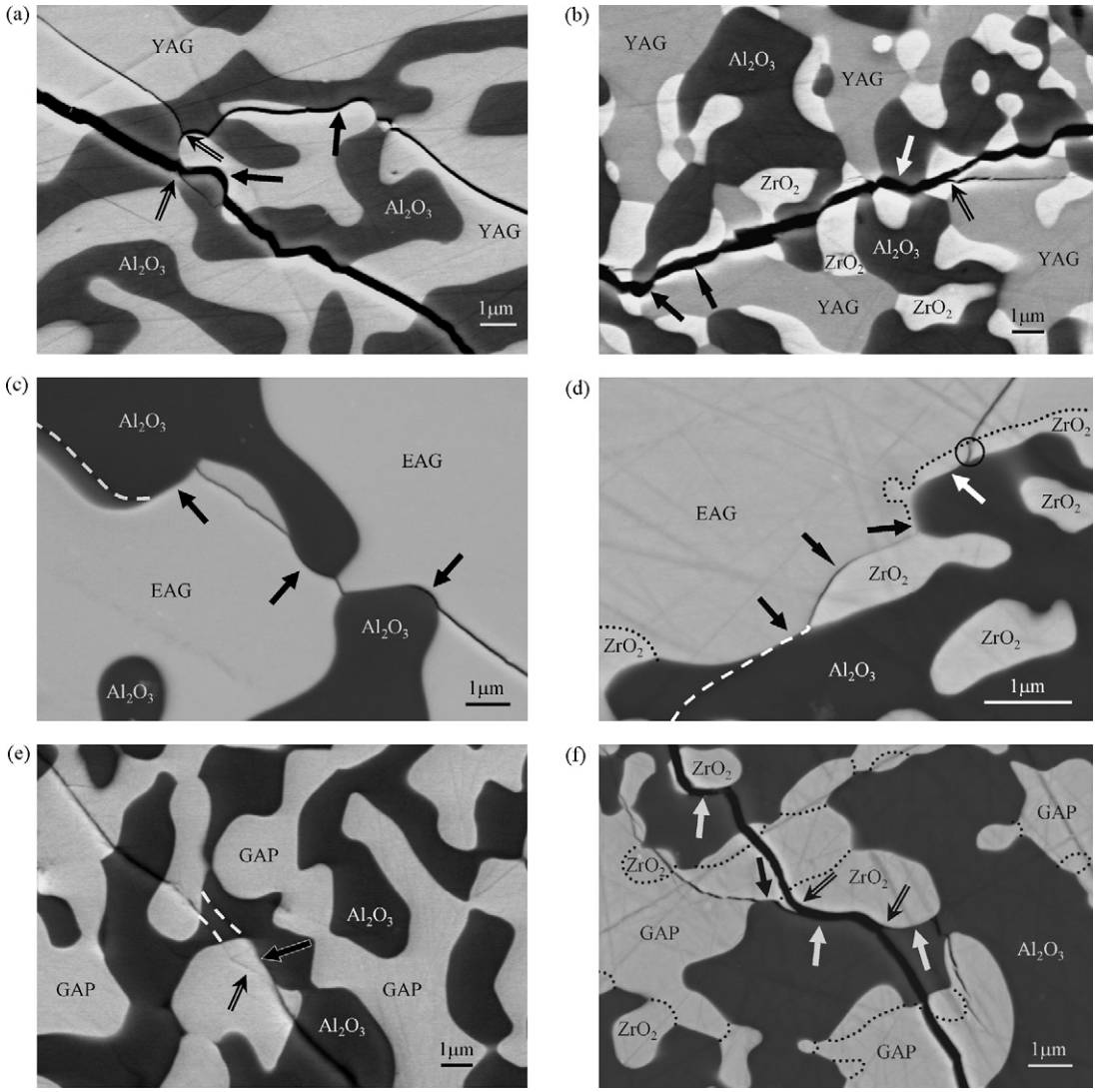

Fig. 2. Crack propagation modes at room temperature in eutectic ceramics subjected to biaxial flexure (FEG-SEM, back-scattered electrons): Al_2O_3/YAG (a), Al_2O_3/YAG/ZrO_2 (b), Al_2O_3/EAG (c), Al_2O_3/EAG/ZrO_2 (d), Al_2O_3/GAP (e) and Al_2O_3/GAP/ZrO_2 (f).

It should be noted that the CTE's of the three ternary eutectics are higher than those of the corresponding binary eutectics. This phenomenon may be attributed to the presence of Y_2O_3-, Er_2O_3- and Gd_2O_3-doped ZrO_2. In each case, the percentage of dopant is rather high (≈20 mol%).[19] X-ray diffraction tests and transmission electron microscopy examinations have shown that the ZrO_2 phases are stabilized zirconia having a cubic (fcc) structure. The CTE's of such doped ZrO_2 are markedly higher[8] than that of pure ZrO_2. The fact that the CTE's of the doped ZrO_2 are higher than those of the binary eutectics, explains the higher values of the CTE's of the ternary eutectics, as compared with the binary eutectics.

Concerning the determination of the Young's moduli of the various eutectic composites through compression tests, measurements performed on Al_2O_3 single crystals have already demonstrated the feasibility of the method. Although the measurements performed on the eutectic composites may only be considered as preliminary tests, they seem to confirm the result previously found on the Al_2O_3/YAG binary eutectic composite,[4] where the measured Young's modulus corresponds to that given by the rule of mixture.

4. Discussion

The various crack propagation modes observed using the biaxial bending tests must be correlated to internal thermal stress measurements and calculations. First of all, it should be noted that the microstructure is only locally lamellar in some rare areas, but is rather hieroglyphic in shape with numerous convex phase boundaries. The arrangement of the various phases can thus no more be represented by a stacking of plates. In this context, the presence of ZrO_2 phases surrounded by a continuous layer of Al_2O_3 (Fig. 2d; top right corner) and Fig. 2f (top left corner) suggests the use of a model of concentric cylinders (Fig. 4a). Contrary to the model of stacked plates, this model allows the determination of the normal stresses acting on the interfaces between the various phases and resulting from this type of concentric arrangement. These normal stresses are given

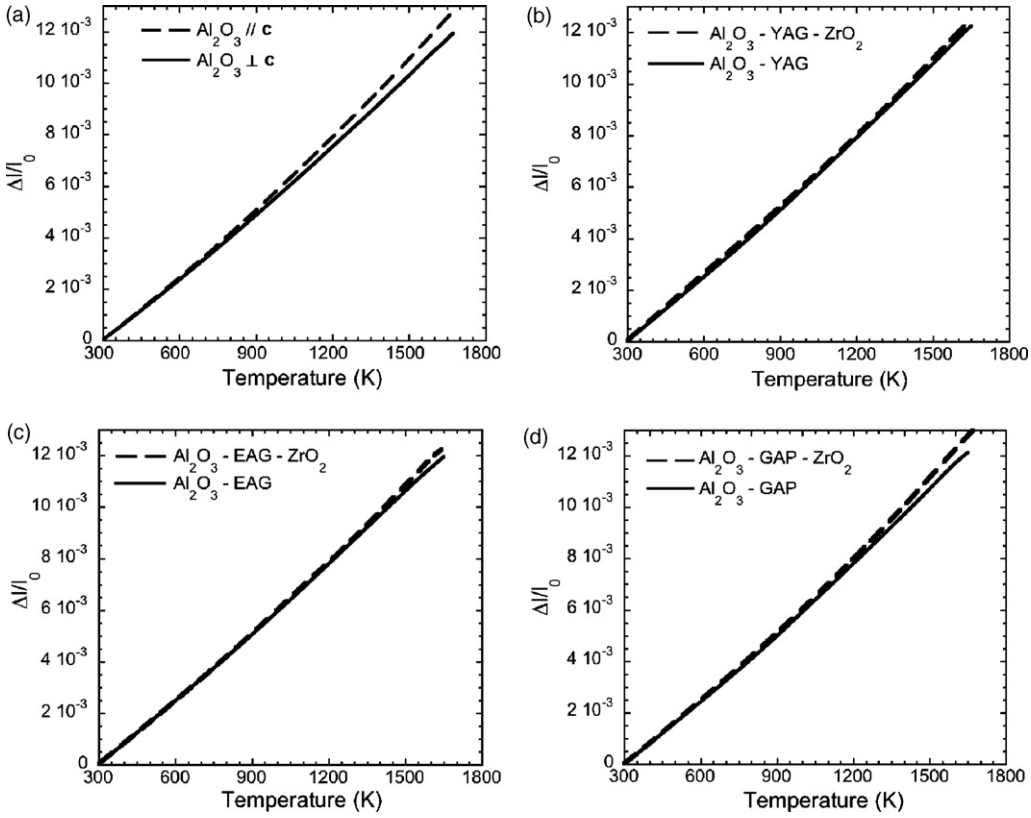

Fig. 3. Thermal expansion (strain *vs.* temperature curves, the coefficients of thermal expansion being given by the slope of the curves) of Al_2O_3 single crystals (directions // and $\perp$ *c*) and of the investigated eutectic ceramics (longitudinal direction).

by the value of the radial stress component (σ_r) at the interface under consideration. For instance, the ZrO_2 phases in Fig. 2d (top right corner) and f (top left corner) may be represented by a 1 μm in diameter ZrO_2 bar, bonded into a 1.5 μm in thickness Al_2O_3 sleeve, surrounded by 0.5 μm in thickness ZrO_2 sleeve, these three concentric cylinders being embedded into an equivalent homogeneous medium (EHM) having the diameter of the specimen under investigation and the macroscopic thermomechanical properties of the bulk Al_2O_3/EAG/ZrO_2 or Al_2O_3/GAP/ZrO_2 eutectics, respectively. In the present case of only four concentric phases subjected to a temperature change ($\Delta T \approx 1700\,^{\circ}C$), a completely analytical solution is obtained[22]; the values of the stress components in the various phases and interfaces may thus be directly calculated through these formulae. In the case of the Al_2O_3/GAP/ZrO_2 eutectics, the normal stress acting on the ZrO_2/Al_2O_3 interface attains ≈1000 MPa (Fig. 4b); this high tensile normal stress helps interface crack propagation, as observed in Fig. 2f (top left corner). The external ZrO_2 layer is subjected to a high tensile circumferential loading ($\sigma_\theta \approx 1800$ MPa) which helps transgranular crack propagation in these phases, as observed in Fig. 2d (circle, top right corner) and f (top left corner). Due to the fact that this model of concentric cylinders is only a crude representation of the real geometrical configuration, such values can only be considered as

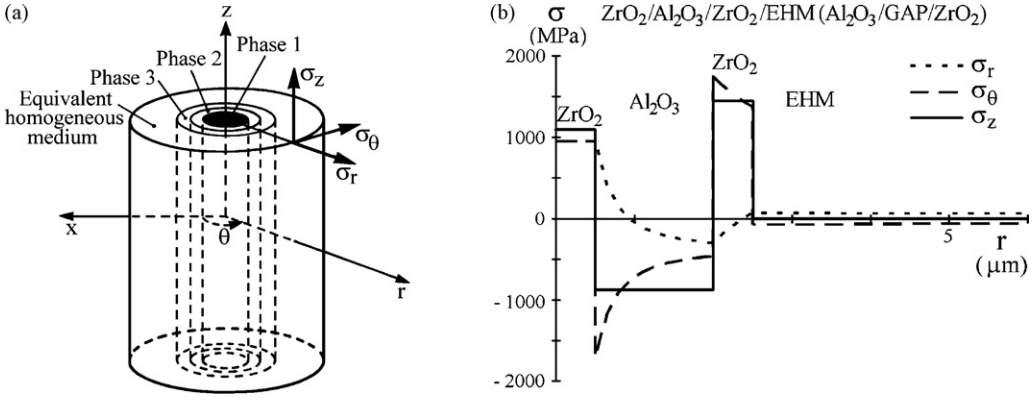

Fig. 4. Internal thermal stresses. Determination of the normal stress component acting on the phase boundaries. The four-phase concentric cylinder model (a) and the corresponding stress system (b), where σ_n is given by the radial stress component σ_r.

estimates. However, as compared to the ultimate tensile strength of such eutectic ceramics,[2,7] the level of these internal thermal stress components is very high, which may explain their essential role in crack nucleation and propagation. Determination, through this model, of the normal stress acting on the interfaces thus explains the possibility of crack deviation in the interfaces in the ternary eutectic ceramics. It should also be noted according to this model that a large fraction of the alumina phase is under a compressive loading for the three components (σ_r, σ_θ and σ_z), which is in agreement with internal stress measurements performed on ternary eutectic ceramics.[7] However, in the case of binary eutectic ceramics, the level of the internal thermal stresses is much lower, at least in the case of Al_2O_3/YAG,[5] whereas crack propagation is still observed in the phase boundaries (Fig. 2a–c).

The fact that such a propagation mode is observed essentially along interfaces exhibiting a strong curvature (Fig. 2a–c) suggests the effect of a local weakness of such a curved phase boundary. The two neighbouring phases having given orientations, the crystallographic orientation of the phase boundary with respect to the two phases continuously varies along the curved interface. The nature of the phase boundary (coincidence site lattice and intrinsic dislocation network) thus also continuously varies along the curved interface. Moreover, the radii of curvature may be sufficiently small to isolate half a cylinder of a given phase (Fig. 2a). During cooling, the isolated half-rod and the surrounding material are subjected to strong internal thermal stresses which may be determined through a concentric cylinder model. This stress field may lead to plastic deformation; the resulting dislocations may reach the interface, the impinging dislocations becoming extrinsic dislocations. In this context, an extension of the already performed microstructural investigation of the phase boundaries[23,24] may help verifying these assumptions. Nevertheless, the fact that crack branching through cleavage of the individual eutectic phases is observed after interface propagation through debonding, confirms the high strength of the interfaces.

5. Conclusion

Biaxial bending tests investigation of the crack propagation modes in the directionally solidified eutectics have revealed the possibility of crack deflection through crack propagation in the phase boundaries. Although observed over short distances, this crack propagation mode through interface debonding allows the crack to strongly deviate from its main path. However, the fact that interface propagation concerns only a very small fraction of the whole crack path confirms the relative high strength of the phase boundaries, compared to cleavage of the various phases during transgranular crack propagation. This relative high strength of the interfaces is also confirmed by the fact that crack branching is observed in the interfaces where crack deflection through debonding has occurred, whereas the secondary crack has to propagate through cleavage in the neighbouring phase. Even if such a bifurcation mechanism leads to stopped cracks, it may have a non-negligible role in energy dissipation.

Concerning the fracture toughness of eutectic ceramics, measurements have shown that the fracture toughness increases from the individual constituents to the binary eutectics and to the ternary eutectics.[19,23] In this respect, it should also be noted that the observed crack deflection modes are more numerous in ternary than in binary eutectics, this experimental result is in good agreement with the previously determined improvement of the fracture toughness.

Acknowledgements

The authors would like to thank M. Bejet (design of the biaxial bending testing device), M.-H. Ritti (dilatometric measurements), A. Mavel (compression tests), M. Raffestin (FEG-SEM investigation) and Dr. P. Beauchêne for their kind cooperation and fruitful discussions. L. Perrière would also like to thank the French Defence Research Organization (DGA) for a Doctorate Scholarship.

References

1. Waku, Y., Nakagawa, N., Wakamoto, T., Ohtsubo, H., Shimizu, K. and Kohtoku, Y., A ductile ceramic eutectic composite with high strength at 1873 K. *Nature*, 1997, **389**, 49–52.
2. Waku, Y., Nakagawa, N., Wakamoto, T., Ohtsubo, H., Shimizu, K. and Kohtoku, Y., High temperature strength and stability of unidirectionally solidified Al_2O_3/YAG eutectic composite. *J. Mater. Sci.*, 1998, **33**, 1217–1225.
3. Dickey, E. C., Frazer, C. S., Watkins, T. R. and Hubbard, C. R., Residual stresses in high temperature ceramic eutectics. *J. Eur. Ceram. Soc.*, 1999, **19**, 2503–2509.
4. Suzuki, H., Akita, K., Yoshioka, Y., Waku, Y. and Misawa, H., Evaluation of phase stresses of Al_2O_3/YAG binary MGC by synchrotron radiation—Residual stress states and stress behavior of YAG phase. *J. Soc. Mater. Sci. Jpn.*, 2003, **52**, 770–775.
5. Torii, S., Kamiyama, T., Oikawa, K., Waku, Y. and Fukunaga, T., Strain measurement of the directionally solidified eutectic $Al_2O_3/Y_3Al_5O_{12}$ (YAG) ceramic by neutron diffraction. *J. Eur. Ceram. Soc.*, 2005, **25**, 1307–1311.
6. Gouadec, G., Colomban, Ph., Piquet, N., Trichet, M. F. and Mazerolles, L., Raman/Cr^{3+} fluorescence mapping of a melt-grown $Al_2O_3/GdAlO_3$ eutectic. *J. Eur. Ceram. Soc.*, 2005, **25**, 1447–1453.
7. Peña, J. I., Larson, M., Merino, R. I., de Francisco, I., Orera, V. M., Llorca, J. *et al.*, Processing, microstructure and mechanical properties of directionally-solidified Al_2O_3-$Y_3Al_5O_{12}$-ZrO_2 ternary eutectics. *J. Eur. Ceram. Soc.*, 2006, **26**, 3113–3121.
8. Adams, J. W., Nakamura, H. H., Ingel, R. P. and Rice, R. W., Thermal expansion behavior of single-crystal zirconia. *J. Am. Ceram. Soc.*, 1985, **68**, C228–C231.
9. Ingel, R. P. and Lewis III, D., Elastic anisotropy in zirconia single-crystals. *J. Am. Ceram. Soc.*, 1988, **71**, 265–271.
10. Goto, T., Anderson, O. L., Ohno, I. and Yamamoto, S., Elastic constants of corundum up to 1825 K. *J. Geophys. Res.*, 1989, **94**, 7588–7602.
11. Gupta, T. K. and Valentich, J., Thermal expansion of yttrium aluminium garnet. *J. Am. Ceram. Soc.*, 1971, **54**, 355–356.
12. Alton, W. J. and Barlow, A. J., Temperature dependence of the elastic constants of yttrium aluminium garnet. *J. Appl. Phys.*, 1967, **38**, 3023–3024.
13. Ochiai, S., Ueda, T., Sato, K., Hojo, M., Waku, Y., Sakata, S. *et al.*, Elastic modulus and coefficient of thermal expansion of Al_2O_3/YAG composite at room to ultra high temperatures. *Mater. Sci. Res. Intern., Spec. Tech. Publ.*, 2001, **2**, 281–285.
14. Levin, E. M. and McMurdie, H. F., *Phase Diagrams for Ceramists (1975 Supplement)*. The American Ceramic Society, Columbus, OH, 1975, pp. 131–132.
15. Mizuno, M., Phase diagrams of the systems Al_2O_3-Ho_2O_3 and Al_2O_3-Er_2O_3 at high temperatures. *Yogyo Kyokai Shi*, 1979, **87**, 405–412.

16. Mizuno, M., Yamada, T. and Noguchi, T., Phase diagrams of the systems Al_2O_3-Eu_2O_3 and Al_2O_3-Gd_2O_3 at high temperatures. *Yogyo Kyokai Shi*, 1977, **85**, 543–548.
17. Lakiza, S. M. and Lopato, L. M., Stable and metastable phase relations in the system alumina-zirconia yttria. *J. Am. Ceram. Soc.*, 1997, **80**, 893–902.
18. Waku, Y., Sakata, S., Mitani, A. and Shimizu, K., High-temperature strength and a microstructure of an Al_2O_3/$Er_3Al_5O_{12}$/ZrO_2 ternary MGC. *J. Jpn. Inst. Met.*, 2000, **64**, 1263–1268.
19. Piquet, N., Microstructures interconnectées dans des eutectiques à base d'oxydes réfractaires élaborés par solidification dirigée. Doctorate thesis. University Paris XII, 2006.
20. Vitman, F. F., Bartenev, G. M., Pukh, V. P. and Tsepkov, L. P., A method for measuring the strength of sheet glass. *Glass Ceram. (Steklo i Keramika)*, 1962, **19**, 412–414.
21. Schmitt, R. W., Blank, K. and Schönbrunn, G., Experimentelle Spannungsanalyse zum Doppelringverfahren. *Sprechsaal*, 1983, **116**, 397–405.
22. Brunet, A., Valle, R. and Vassel, A., Intermetallic TiAl-based matrix composites: investigation of the chemical and mechanical compatibility of a protective coating adapted to an alumina fibre. *Acta Mater.*, 2000, **48**, 4763–4774.
23. Mazerolles, L., Piquet, N., Trichet, M. F. and Parlier, M., Microstructures and interfaces in melt-growth Al_2O_3-Ln_2O_3 based eutectic composites. *Adv. Sci. Technol.*, 2006, **45**, 1377–1384.
24. Mazerolles, L., Perrière, L., Lartigue-Korinek, S., Piquet, N. and Parlier, M., Microstructures, crystallography of interfaces and creep behaviour of melt-growth composites. *J. Eur. Ceram. Soc.*, doi:10.1016/j.jeurceramsoc.2008.01.014, in press.